Title

Engineering high-level production of fatty alcohols by Saccharomyces cerevisiae from lignocellulosic feedstocks

Authors

d'Espaux, Leo

Ghosh, Amit

Runguphan, Weerawat

et al.

Publication Date

2017-07-01

DOI

10.1016/j.ymben.2017.06.004

Peer reviewed

Metabolic Engineering 42 (2017) 115–125

Contents lists available at ScienceDirect

Metabolic Engineering

journal homepage: www.elsevier.com/locate/meteng

Engineering high-level production of fatty alcohols by *Saccharomyces cerevisiae* from lignocellulosic feedstocks

Leo d'Espaux[a,b], Amit Ghosh[a,b,1], Weerawat Runguphan[a,b,2], Maren Wehrs[a,b], Feng Xu[a,b,c,d], Oliver Konzock[a,b], Ishaan Dev[a,b,e], Melissa Nhan[a,b,3], Jennifer Gin[a,b], Amanda Reider Apel[a,b], Christopher J. Petzold[a,b], Seema Singh[a,b,c,d], Blake A. Simmons[a,b,c,d], Aindrila Mukhopadhyay[a,b], Héctor García Martín[a,b], Jay D. Keasling[a,b,e,f,g,*]

[a] *DOE Joint BioEnergy Institute, Emeryville, CA 94608, United States*
[b] *Biological Systems and Engineering Division, Lawrence Berkeley National Laboratory, Berkeley, CA 94720, United States*
[c] *Biomass Science and Conversion Technology Department, Sandia National Laboratories, Livermore, CA 94551, United States*
[d] *Biological and Materials Science Center, Sandia National Laboratories, Livermore, CA 94551, United States*
[e] *Department of Chemical & Biomolecular Engineering, University of California, Berkeley, CA 94720, United States*
[f] *Department of Bioengineering, University of California, Berkeley, CA 94720, United States*
[g] *The Novo Nordisk Foundation Center for Sustainability, Technical University of Denmark, Denmark*

ABSTRACT

Fatty alcohols in the C12-C18 range are used in personal care products, lubricants, and potentially biofuels. These compounds can be produced from the fatty acid pathway by a fatty acid reductase (FAR), yet yields from the preferred industrial host *Saccharomyces cerevisiae* remain under 2% of the theoretical maximum from glucose. Here we improved titer and yield of fatty alcohols using an approach involving quantitative analysis of protein levels and metabolic flux, engineering enzyme level and localization, pull-push-block engineering of carbon flux, and cofactor balancing. We compared four heterologous FARs, finding highest activity and endoplasmic reticulum localization from a *Mus musculus* FAR. After screening an additional twenty-one single-gene edits, we identified increasing FAR expression; deleting competing reactions encoded by *DGA1*, *HFD1*, and *ADH6*; overexpressing a mutant acetyl-CoA carboxylase; limiting NADPH and carbon usage by the glutamate dehydrogenase encoded by *GDH1*; and overexpressing the Δ9-desaturase encoded by *OLE1* as successful strategies to improve titer. Our final strain produced 1.2 g/L fatty alcohols in shake flasks, and 6.0 g/L in fed-batch fermentation, corresponding to ~ 20% of the maximum theoretical yield from glucose, the highest titers and yields reported to date in *S. cerevisiae*. We further demonstrate high-level production from lignocellulosic feedstocks derived from ionic-liquid treated switchgrass and sorghum, reaching 0.7 g/L in shake flasks. Altogether, our work represents progress towards efficient and renewable microbial production of fatty acid-derived products.

1. Introduction

Several laboratories have reported on engineering the fatty acid pathway in a microbial host such as *Saccharomyces cerevisiae* as a sustainable platform for producing biofuels and other products (Kalscheuer et al., 2006; Runguphan and Keasling, 2013). A range of enzymes and pathways have been heterologously expressed to convert fatty acid thioesters—produced by endogenous fatty acid biosynthesis—into ethyl esters, acids, alcohols, alkanes, methyl ketones, dicarboxylic acids, etc. (Clomburg et al., 2015; Goh et al., 2012; Zhou et al., 2016). Among these products, long-chain fatty alcohols in the C12-C18 range have recently received intense attention due to their value and broad applications in laundry detergents, industrial lubricants and surfactants, medicines and personal care products, and potentially as biofuels (Feng

* Correspondence to: Joint BioEnergy Institute, 5885 Hollis St., Emeryville, CA 94608, United States.
E-mail address: jdkeasling@lbl.gov (J.D. Keasling).
[1] Present address: School of Energy Science and Engineering, Indian Institute of Technology, Kharagpur 721302, India.
[2] Present address: Microbial Cell Factory Laboratory, National Center for Genetic Engineering and Biotechnology, National Science and Technology Development Agency, Pathum Thani, Thailand.
[3] Present address: Calysta Energy, Menlo Park, CA 94025, United States.

http://dx.doi.org/10.1016/j.ymben.2017.06.004
Received 27 April 2017; Received in revised form 26 May 2017; Accepted 5 June 2017
Available online 10 June 2017
1096-7176/ Published by Elsevier Inc. on behalf of International Metabolic Engineering Society.

et al., 2015; Liu et al., 2016; Pfleger et al., 2015). In 2016, the worldwide market for fatty alcohols was $3.7 billion and growing, with annual production of more than 2.6 metric tons sourced primarily from fossil fuels (petroleum, or polymerized natural gas) or plant oil crops (triglycerides) processed chemically into alcohols (Gaikwad, 2016). Microbial production, besides providing a more sustainable source, can allow for highly specific chemical modifications (Haushalter et al., 2014) to improve product performance or create new applications in ways that could be difficult or impossible by traditional thermochemical means.

However, low yields and economic competition from mature petrochemical processes hamper widespread adoption of microbial fatty alcohol production. Traditionally, *S. cerevisiae* is the preferred industrial biorefinery host due to its genomic and structural robustness, and since existing ethanol-producing fermentation facilities could be retrofitted for another product. Yet yields of fatty alcohols in *S. cerevisiae* stand at less than 2% of the theoretical maximum from glucose (Zhou et al., 2016). Besides product yield, economic viability also depends on the choice of feedstocks. Sugars derived from food crops are cost-prohibitive and divert water and other resources in a period where demand for food and water is expected to increase ~ 50% by the turn of this century (Connor and Uhlenbrook, 2016). Using lignocellulosic feedstocks derived from agricultural waste or energy crops that do not compete for water and land with food would lower costs and provide maximal CO_2 emission offsets (Caspeta and Nielsen, 2013).

In this work, we improved titers and yields of fatty alcohols produced by *S. cerevisiae* and demonstrated high-level production from lignocellulosic biomass hydrolysates. Our approach included quantitative analysis of metabolic flux and global protein expression to identify pathway bottlenecks in a first-generation fatty chemical producer strain and identify genetic modifications for maximizing pathway flux. Among these modifications, we compared four heterologous fatty acid reductases—which convert fatty acyl-CoA into fatty alcohols—exploring enzyme expression level and subcellular localization. Additionally, we screened over two dozen genetic modifications for improvements in fatty alcohol production and combined beneficial changes into a strain that produced fatty alcohols at high titers and yields. To develop an efficient bioprocess with our strain, we evaluated fatty alcohol production from lignocellulosic feedstocks in a one-pot process using cholinium-based ionic liquids. Lastly, we demonstrated successful scale-up in 2 L fed-batch bioreactors combined with an initial exploration of alternative substrate feeding strategies to maximize titer and yield.

2. Materials and methods

2.1. Generating strains

All yeast strains in this study are derived from Saccharomyces cerevisiae BY4741 (Brachmann et al., 1998), to which we replaced the native promoters driving ACC1, FAS1, and FAS2 with the TEF1 promoter as previously reported, generating strain WRY1 (Runguphan and Keasling, 2013). All subsequent strains (Table 1) were created via Cas9-aided homologous recombination using the software tool CASdesigner (casdesigner.jbei.org) to design integration cassettes and following a previously reported, cloning-free methodology (Reider Apel et al., 2016). Briefly, integration cassettes containing 1-kb flanking homology regions targeting a chosen genomic locus were constructed by PCR-amplifying donor DNA fragments using primers generated by CASdesigner, then co-transformed with a Cas9-gRNA plasmid (pCut) targeting the chosen genomic locus. CASdesigner primers provide 30–60 nt of inter-fragment homology allowing 1–5 separate fragments to assemble via homologous recombination in vivo. pCuts targeting empty genomic loci (e.g., 208a, 1622b) were available pre-cloned, and pCuts targeting new sites (e.g., for deletions) were assembled in vivo from a linear backbone and a linear PCR fragment containing the new gRNA sequence, as described previously (Reider Apel et al., 2016). New gRNA sequences (Suppl. Table 1) were chosen using DNA2.0 (www.dna20.com/eCommerce/cas9/input) or CHOP-CHOP (chopchop.rc.fas.harvard.edu) (Montague et al., 2014). To generate donor DNA fragments, native sequences—e.g., chromosomal homology regions, promoters—were amplified from BY4741 genomic DNA, while heterologous sequences—e.g., fatty acid reductase coding sequences (Suppl. Table 2)—were amplified from synthetic gene blocks codon-optimized (for expression in *S. cerevisiae*) and synthesized by Integrated DNA Technologies (www.idtdna.com). All PCRs used Phusion Hot Start II DNA polymerase (www.thermofisher.com, cat. F549L).

Transformations were performed via heat-shock (Gietz and Woods, 2002) using ~ 200 ng pCut, ~ 1 μg donor DNA per sample, and 20 min heat shock. For assembling a pCut targeting a new site by homologous recombination, we used 200 ng linear pCut backbone and 500 ng of a 1-kb fragment containing the gRNA sequence, as described (Reider Apel et al., 2016). For multi-site integrations, we used 200 ng total linear pCut backbone, and the same amounts of gRNA fragment and donor DNA for each site as we would have for a single integration. Colonies were screened by PCR directed at the target locus, and for integrations, one representative colony sequenced. Three to four biological replicates were analyzed for each strain.

2.2. Media and culture conditions

Selective agar plates used for transformations were purchased from Teknova (www.teknova.com, cat. C3080). Liquid selective medium used to grow transformants contained 0.2% (w/v) complete supplement mixture (CSM) lacking uracil (www.sunrisescience.com, cat. 1004-100), 0.67% yeast nitrogen base (www.difco.com, cat. 291920), and 2% dextrose. Nonselective medium contained 1% yeast extract, 2% peptone (Difco cat. 288620 and 211677, respectively), and either 2% dextrose (YPD) or 2% galactose and 0.2% dextrose (YPG). Nonselective agar YPD plates were purchased from Teknova (cat. Y100). Cultures were grown in plastic 96-deep well plates (www.vwr.com, cat. 29445-166), 24-deep well plastic plates (CWR cat. 89080-534), glass test tubes, or 250-ml baffled flasks, as indicated in the results section. Production cultures were overlaid with dodecane (www.sigma.com, cat. D221104), the latter spiked with 200 mg/L methyl nonadecanoate (sigma cat. N5377) as an internal standard. Plastic plates were covered with aeraseal film (www.excelscientific.com, cat. BS-25) and shaken at 800 rpm in a Multitron shaker (www.infors-ht.com, model AJ185). Glass tubes and baffled flasks were shaken at 200 rpm. All strains were grown at 30 °C.

2.3. Shotgun proteomics

Strains for proteomics analysis were grown in YPD overnight, then back-diluted 1:100 into 5 ml fresh YPD and grown 8 h. For each sample, the entire culture volume was centrifuged at 3000 × *g* on a table-top centrifuge, decanted, and the pellet flash-frozen in liquid nitrogen and stored at −80 °C until preparation as described (Batth et al., 2012). Briefly, cell pellets were lysed in urea and bead-beaten. The lysate was reduced using tris(2-carboxyethyl)phosphine (sigma cat. C4706), then alkylated using iodoacetamide (sigma cat. I1149), trypsinized, desalted on spin columns (www.harvardapparatus.com, cat. 74–4101), and finally suspended in a buffer of 0.1% formic acid to a final concentration of 2 μg protein/μl. Peptide data were acquired using an Agilent 1290 liquid chromatography system coupled to an Agilent 6550 QTOF mass spectrometer and analyzed using Agilent MassHunter version B.06.00 (www.agilent.com). Resultant data files were searched with Mascot version 2.3.02 (www.matrixscience.com) then filtered and validated using Scaffold version 4.4.0 (www.proteomesoftware.com).

Table 1
Strains. The following strains used in this study are available from the JBEI registry (https://public-registry.jbei.org/folders/322).

Strain	*yL#*	*Parent (additional genetic changes)*	*Reference*
BY4741	7	MATa, his3Δ1, leu2Δ0, met15Δ0, ura3Δ0	Runguphan and Keasling, 2013
WRY1	400	BY4741 (acc1::P_{TEF1}-ACC1, fas1::P_{TEF1}-FAS1, fas2::P_{TEF1}-FAS2)	Runguphan and Keasling, 2013
TesA	401	WRY1 (208a::P_{TEF1}-EcTesAcyt-T_{CYC1}, faa1Δ, faa4Δ)	This work
MaFAR2	402	WRY1 (208a::P_{TEF1}-MaFAR2-T_{CYC1})	This work
MaFAR7	403	WRY1 (208a::P_{TEF1}-MaFAR7-T_{CYC1})	This work
TaFAR1	404	WRY1 (208a::P_{TEF1}-TaFAR1-T_{CYC1})	This work
MmFAR1	405	WRY1 (208a::P_{TEF1}-MmFAR1-T_{CYC1})	This work
FAR	406	yL405 (1622b::P_{GAL1}-MmFAR1-T_{TDH1})	This work
FAR-GFP	407	yL405 (1622b::P_{GAL1}-MmFAR1-GFP-T_{TDH1})	This work
MBP-FAR	408	yL405 (1622b::P_{GAL1}-MBP-MmFAR1-T_{TDH1})	This work
MBP-FAR-GFP	409	yL405 (1622b::P_{GAL1}-MBP-MmFAR1-GFP-T_{TDH1})	This work
ACC1**	410	yL405 (YPRCd15c::P_{GAL1}-ACC1**-T_{ENO2})	This work
HFA1cyt	411	yL405 (YPRCd15c::P_{GAL1}-HFA1cyt-T_{ENO2})	This work
dga1Δ	412	yL405 (dga1Δ)	This work
lro1Δ	413	yL405 (lro1Δ)	This work
are2Δ	414	yL405 (are2Δ)	This work
are1Δ	415	yL405 (are1Δ)	This work
pxa1Δ	416	yL405 (pxa1Δ)	This work
pox1Δ	417	yL405 (pox1Δ)	This work
hfd1Δ	418	yL405 (hfd1Δ)	This work
adh6Δ	419	yL405 (adh6Δ)	This work
tdh3Δ::BcGapN	420	yL405 (tdh3Δ::BcGapN)	This work
tdh3Δ::KlGapDH	421	yL405 (tdh3Δ::KlGapDH)	This work
pgi1Δ::ZWF1	422	yL405 (pgi1Δ::ZWF1)	This work
gdh1Δ	423	yL405 (gdh1Δ)	This work
OLE1	424	yL405 (1014a::P_{TEF2}-OLE1-T_{ADH1})	This work
opi1Δ::INO2	425	yL405 (opi1Δ::P_{TPI1}-INO2-T_{PGK1})	This work
rpd3Δ	426	yL405 (rpd3Δ)	This work
2RA	427	yL406 (YPRCd15c::P_{GAL1}-ACC1**-T_{ENO2})	This work
2RAh	428	yL427 (hfd1Δ)	This work
2RAha	429	yL427 (hfd1Δ, adh6Δ)	This work
2RAhag	430	yL427 (hfd1Δ, adh6Δ, gdh1Δ)	This work
3RAhag	431	yL430 (1114a::P_{GAL1}-MmFAR1-T_{TDH1})	This work
2RAhagd	432	yL430 (dga1Δ)	This work
2RAhagdO	433	yL430 (dga1Δ, 1014a::P_{TEF2}-OLE1-T_{ADH1})	This work
2RAhagdOG	434	yL433 (gal80Δ::P_{TDH3}-GAL4)	This work

2.4. Metabolic flux analysis using ^{13}C-labeled glucose

Metabolic flux analysis was performed as previously reported (García Martín et al., 2015; Ghosh et al., 2016). Briefly, strains were grown in 250-ml shake flasks in 25 ml medium containing ^{13}C-labeled glucose (sigma cat. 407-622-22-9 and 110187-42-3) and sampled at exponential phase near OD 1.0. Sampling included filtering media for high-performance liquid chromatography (HPLC) to quantify extracellular metabolites, ethyl acetate extraction followed by gas chromatography-mass spectrometry (GC-MS) to quantify fatty acid products, and methanol/chloroform extraction followed by liquid chromatography–mass spectrometry (LC-MS/MS) to analyze ^{13}C labeling in metabolites. These ^{13}C labeling data were used to constrain the *S. cerevisiae* genome-scale model iMM904 (Mo et al., 2009) using two-scale ^{13}C Metabolic Flux Analysis (García Martín et al., 2015; Ghosh et al., 2016) with the open-source, python-based JBEI Quantitative Metabolic Modeling library (https://github.com/JBEI/jqmm) to model the metabolic flux distribution.

2.5. Fatty alcohol production cultivations

Initial production cultivations were performed as described (Runguphan and Keasling, 2013). Briefly, three to four biological replicates were each inoculated into 5 ml medium in glass test tubes overnight, then back-diluted 1:100 into 5 ml of the same medium, overlaid with 0.5 ml dodecane (spiked with internal standard), and shaken at 200 rpm for three days. The overlay was collected and centrifuged at 3000 × *g*, and 10 µl of the top organic phase added to 90 µl ethyl acetate in a GC-MS vial containing a glass insert for subsequent analysis. This method of cultivation and sampling was used to compare the fatty acid reductases, in YPD, and for initial cultivations of strain yL405 in biomass hydrolysates and other media.

To screen genetically edited strains for improvements in fatty alcohol production, the appearance of precipitated fatty alcohols in some strains (producing > 800 mg/L, e.g., Fig. 3C) prevented sampling the liquid overlay. Instead, four biological replicates were inoculated into 1 ml YPG in 24-deep well plates and grown overnight, then back-diluted 1:100 into 1 ml YPG, overlaid with 0.2 ml dodecane (spiked with internal standard), covered with aeraseal, and shaken at 800 rpm for three days. Then, 100 µl of culture was added to 800 µl ethyl acetate in 1.6-ml eppendorf tubes, vortexed at maximum setting 30 min, centrifuged at 10,000 × *g* on a table-top centrifuge, and 100 µl of the top organic phase added to a GC-MS vial containing a glass insert for analysis. This method of cultivation and sampling was used to compare strain yL405 to all subsequent genetically modified strains.

To characterize production of the final highest-producer strain yL434, four biological replicates were grown in 1 ml corresponding medium overnight in glass test tubes, then back-diluted 1:100 into 10 ml of the same medium in 250-ml baffled flasks, overlaid with 2 ml dodecane (spiked with internal standard), and shaken at 200 rpm for three days. Then, 100 µl culture was extracted with ethyl acetate and processed into GC-MS vials as described immediately above. This method of cultivation and sampling was used to compare production of yL434 in YPG, YPD, and YPBiomass media (see Preparation of biomass hydrolysates).

2.6. Fed batch 2L-scale bioreactor fermentations

Fed-batch fermentations were performed in Sartorius 2 L bioreactors equipped Sartorius BIOSTAT B Plus control units at the

Advanced Biofuels Process Demonstration Unit (ABPDU, Lawrence Berkeley National Laboratory, Emeryville, CA). The seed strain was inoculated in 500 ml YPD in a 1-L flask and grown overnight to an OD of 4.3. Each bioreactor was loaded with 900 ml YPD, 100 ml inoculum, and 200 ml dodecane (spiked with internal standard). Temperature was maintained at 30 °C via water flow through the reactor jacket. The pH was maintained at 5.0 by auto-dispensing a base solution (2 N NH_4OH). Dissolved oxygen was maintained at 20% via stirring from 400 to 800 rpm (primary cascade), then sparging air from 1 vvm (volume of air per volume of liquid per minute) to 1.5 vvm (secondary cascade). The feed contained 500g/L glucose, 10g/L yeast extract, 10g/L $(NH_4)_2SO_4$, 8g/L KH_2PO_4, 4g/L $MgSO_4$, 0.8g/L NaCl, and 0.5g/L $CaCl_2$ and was added as described in the results section.

2.7. GC-MS and extracellular metabolite analysis

Samples for GC-MS analysis of fatty alcohol content were analyzed on an Agilent 7890A GC equipped with an Agilent 5975 MS detector and an Agilent DB-5MS column. The inlet was set to 250 °C, flow at 1 ml/min; the oven to 150 °C for 2 min, then ramped at 30 °C/min to 250 °C, and held for 2 min. The solvent delay was set to 4 min (or as required to avoid the dodecane peak). An authentic hexadecanol standard (Sigma catalog W255408) was used to determine titer. Extracellular metabolites were analyzed on an automated photometric Gallery Analyzer (www.thermofisher.com, model BR71394) following the manufacturer's instructions.

2.8. Preparation of biomass hydrolysates using renewable liquids

Switchgrass (*Panicum virgatum*) and sorghum (*Sorghum bicolor*) were kindly provided by Idaho National Laboratory. The air-dried biomass was milled (www.thomassci.com, model 3383L40) using a 40-mesh screen (www.ahthomas.com, model 3383-L10), sieved to the nominal sizes of 40–60 mesh (250–400 μm), and air-dried until the moisture was < 10%. The resulting biomass was converted into fermentable sugars in a one-pot, two-step process consisting of biomass pretreatment using cholinium-based IL followed by enzymatic hydrolysis, modified from a previously reported procedure (F. Xu et al., 2016). Briefly, 20 g dry biomass was mixed with an IL solution containing 20 g IL and 160 g water. The ILs used were cholinium lysinate, cholinium alpha-ketoglutarate, or cholinium aspartate. The 200-g mixture was thoroughly mixed and loaded in a 500-ml Parr reactor and heated to 140 °C for 3 h. The reactor was then cooled to room temperature using cooling water, and all the pretreated biomass slurry transferred to a filter membrane for solid-liquid separation. The solid fraction was collected, mixed with distilled water, and pH-adjusted to 5 with HCl. The weight of the mixture after pH adjustment was adjusted to 200 g with distilled water, and all the content transferred into a 1-L shake flask for saccharification. The saccharification was carried out at 50 °C and pH 5 using Novozymes enzyme mixtures Cellic® CTec2 and HTec2, with an enzyme dosage of 20 mg protein per gram glucan and 2 mg protein per gram xylan, respectively. The resulting slurry was filtered using a 0.2-μm filter and used to dissolve 10 g/L yeast extract and 20-g/L peptone, making yeast extract-peptone-biomass hydrolysate media. In the results, YPBiomass refers to sorghum treated with cholinium aspartate.

2.9. Microscopy

Strains for microscopy were grown in 5 ml YPD overnight, then back-diluted 1:100 into the same medium and grown 3–6 h at 200 rpm and 30 °C. Then, 1 ml of culture volume was centrifuged at 10,000 × *g* on a table-top centrifuge, washed with 1x water, and imaged using a Zeiss LSM 710 confocal system mounted on a Zeiss inverted microscope (www.zeiss.com) with a 63× objective and processed using Zeiss Zen software.

3. Results and discussion

3.1. Quantitative analysis of metabolic flux and global protein levels in first-generation fatty chemical producer

We began our work with a quantitative analysis of metabolic fluxes and global protein levels to characterize our first-generation fatty chemical producer strain and identify possible strategies to improve production. In our previous report, we replaced the native promoters driving the three fatty acid biosynthetic genes *ACC1*, *FAS1*, and *FAS2* with the strong *TEF1* promoter and added terminal enzymes to produce ~ 100 mg/L fatty alcohols (using a FAR from *Mus musculus*) and ~ 400 mg/L free fatty acids (using the thioesterase *TesA* from *Escherichia coli*, and deleting the fatty acyl-CoA ligases encoded by *FAA1* and *FAA4*) (Runguphan and Keasling, 2013). In this study, we chromosomally integrated *TesA*, expressing it from the *TEF1* promoter, and analyzed the resulting strain, yL401, using metabolic flux analysis and global proteomics to identify bottlenecks in the biosynthetic pathway. Modeling metabolic fluxes allowed us to identify how substrates and cofactors involved in fatty chemical production are used and produced by other cellular processes and thus identify possible targets for genetic modification. Layering global protein expression data on top of the flux analysis allowed us to identify genes whose differential expression may provide clues into cellular responses to the fatty chemical pathway, as well as a check on expression levels of enzymes in the fatty acid biosynthetic pathway, or along metabolic routes we may wish to engineer.

To quantify global protein expression, we performed shotgun proteomics on yL401 as well as its un-engineered parent, BY4741. For both strains, many of the most highly expressed proteins—detected at between ~ 0.5% and ~ 1.4% of total soluble protein—were glycolytic enzymes (Eno2p, Tdh3p, Tdh2p, Eno1p, Pgk1p), heat shock proteins (Ssa1p, Ssa2p, Ssb1p, Ssb2p), translation elongation factors (Yef3p and Tef1p), and alcohol dehydrogenase 1 (Adh1p). As expected, proteins with increased expression in yL401 included the three fatty acid biosynthetic enzymes Acc1p, Fas1p, and Fas2p (expressed chromosomally from the *TEF1* promoter). Neither FAS subunit was detectable in BY4741, yet both reached ~ 0.25% of soluble protein in yL401. Acc1p was also undetectable in BY4741, but in yL401 reached only ~ 0.02% of soluble protein. Strain yL401 also showed increased expression of several ribosomal and translation-initiation proteins (including Rpl3p, Cdc33p, Mnp1p, and Rpl39p), all induced 2–7 fold relative to BY4741 but remaining under 0.05% of total soluble protein. Proteins with decreased expression in yL401 included several amino acyl-tRNA ligases (Grs1p, Gln4p) and interestingly, the retrotransposon Ty1 Gag-Pol protein (which dropped by half from 0.17% of soluble protein in BY4741). Proteins expressed at intermediate levels in both strains included the cytosolic NADP-dependent acetaldehyde dehydrogenase (Ald6p); the other four ALD isoenzymes—two are cytosolic and NAD-dependent, the other two mitochondrial—were either not detected or found at nominal levels (less than 0.05% of total protein). Of pentose phosphate pathway enzymes, we did not detect glucose-6-phosphate dehydrogenase (Zwf1p), the first and rate-limiting enzyme in the pentose phosphate pathway (Thomas et al., 1991), but did observe several other enzymes involved in the pathway, e.g., Gnd1p. None of the enzymes involved in the tricarboxylic acid (TCA) cycle or glyoxylate cycle were detected at appreciable levels. Of amino acid biosynthesis enzymes, glutamate dehydrogenase (GDH) isoenzyme 1 was the most highly expressed at 0.12% of total soluble protein. The full results of our proteomics analysis are available in Supplementary File 2.

To model the metabolic flux distribution in yL401, we measured metabolite levels and ^{13}C labeling patterns and used the JBEI Quantitative Metabolic Modeling library (García Martín et al., 2015) to model flux through genome-scale model iMM904 (Mo et al., 2009), adding fatty acyl thioesterase reactions (EC number 3.1.2.2). The reconstruction shows carbon from glucose mostly following glycolysis, then the pyruvate dehydrogenase (PDH) bypass from pyruvate to

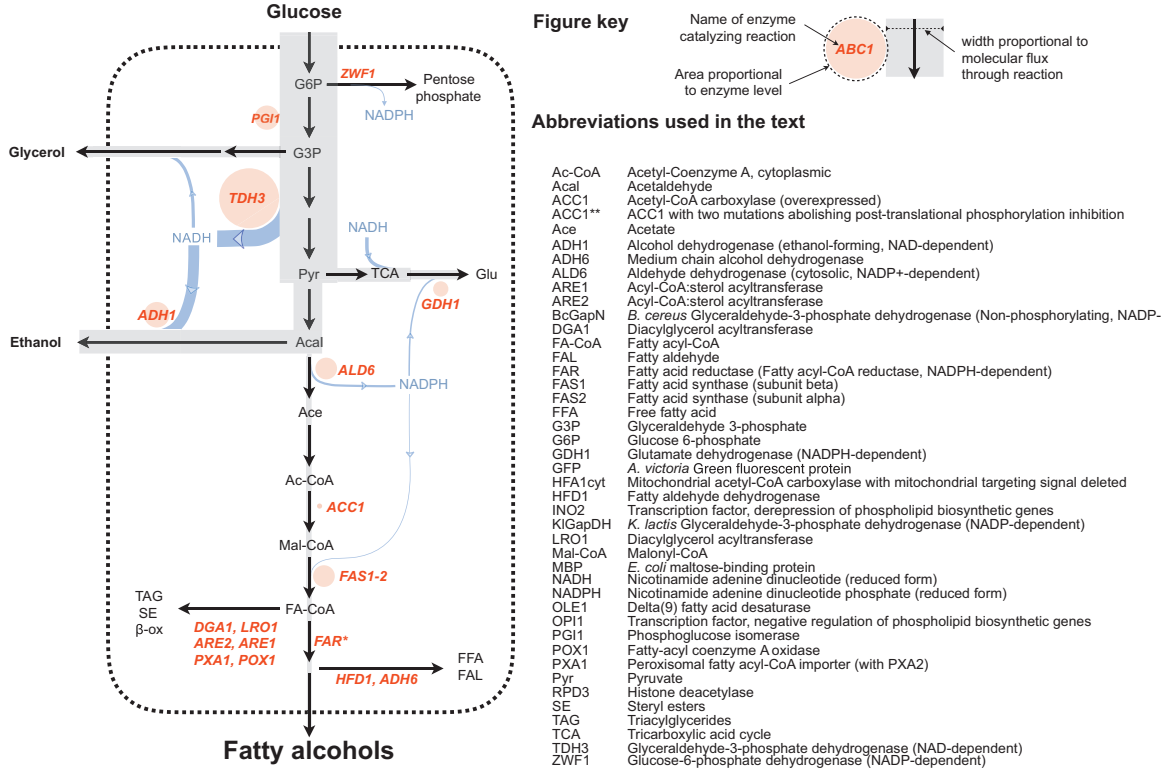

Ac-CoA	Acetyl-Coenzyme A, cytoplasmic
Acal	Acetaldehyde
ACC1	Acetyl-CoA carboxylase (overexpressed)
ACC1**	ACC1 with two mutations abolishing post-translational phosphorylation inhibition
Ace	Acetate
ADH1	Alcohol dehydrogenase (ethanol-forming, NAD-dependent)
ADH6	Medium chain alcohol dehydrogenase
ALD6	Aldehyde dehydrogenase (cytosolic, NADP+-dependent)
ARE1	Acyl-CoA:sterol acyltransferase
ARE2	Acyl-CoA:sterol acyltransferase
BcGapN	*B. cereus* Glyceraldehyde-3-phosphate dehydrogenase (Non-phosphorylating, NADP-
DGA1	Diacylglycerol acyltransferase
FA-CoA	Fatty acyl-CoA
FAL	Fatty aldehyde
FAR	Fatty acid reductase (Fatty acyl-CoA reductase, NADPH-dependent)
FAS1	Fatty acid synthase (subunit beta)
FAS2	Fatty acid synthase (subunit alpha)
FFA	Free fatty acid
G3P	Glyceraldehyde 3-phosphate
G6P	Glucose 6-phosphate
GDH1	Glutamate dehydrogenase (NADPH-dependent)
GFP	*A. victoria* Green fluorescent protein
HFA1cyt	Mitochondrial acetyl-CoA carboxylase with mitochondrial targeting signal deleted
HFD1	Fatty aldehyde dehydrogenase
INO2	Transcription factor, derepression of phospholipid biosynthetic genes
KlGapDH	*K. lactis* Glyceraldehyde-3-phosphate dehydrogenase (NADP-dependent)
LRO1	Diacylglycerol acyltransferase
Mal-CoA	Malonyl-CoA
MBP	*E. coli* maltose-binding protein
NADH	Nicotinamide adenine dinucleotide (reduced form)
NADPH	Nicotinamide adenine dinucleotide phosphate (reduced form)
OLE1	Delta(9) fatty acid desaturase
OPI1	Transcription factor, negative regulation of phospholipid biosynthetic genes
PGI1	Phosphoglucose isomerase
POX1	Fatty-acyl coenzyme A oxidase
PXA1	Peroxisomal fatty acyl-CoA importer (with PXA2)
Pyr	Pyruvate
RPD3	Histone deacetylase
SE	Steryl esters
TAG	Triacylglycerides
TCA	Tricarboxylic acid cycle
TDH3	Glyceraldehyde-3-phosphate dehydrogenase (NAD-dependent)
ZWF1	Glucose-6-phosphate dehydrogenase (NADP-dependent)

Fig. 1. Schema for fatty chemical engineering showing metabolic flux and protein levels of previous first-generation producer. The highest-titer chemical producer strain (yL401) from our previous study (Runguphan and Keasling, 2013) was analyzed by shotgun proteomics (Batth et al., 2012) and metabolic flux analysis (García Martín et al., 2015) to identify targets for engineering increased production. The black dotted line demarcates the cell. Gene names in red indicate targets of our engineering efforts. The area of each red circle is proportional to relative abundance of the named enzyme. The width of each gray line is proportional to the carbon flux through the reaction. The width of each blue line is proportional to flux of reducing equivalents (from NADH or NADPH) through the reaction (not on the same scale molar scale as carbon flux). Fluxes to CO_2, biomass, and minor products are not shown. (For interpretation of the references to color in this figure legend, the reader is referred to the web version of this article).

acetaldehyde, and lastly to ethanol (Fig. 1). At high glucose levels, yeast primarily ferments carbon via the PDH bypass rather than oxidize it via mitochondrial respiration, a well-documented phenomenon known as the Crabtree Effect (Zampar et al., 2013). Branching from central carbon metabolism, our reconstruction shows the metabolic route to our product: some of the acetaldehyde is converted to acetate, then acetyl-CoA, malonyl-CoA, and lastly fatty acyl-CoA and derived chemicals. From acetaldehyde, only ~ 16% of the carbon flux is converted to acetate; the rest to ethanol (by alcohol dehydrogenase, ADH). The production of ethanol is a mechanism to recycle the large flux of NADH produced by glyceraldehyde-3-phosphate dehydrogenase (GapDH), since respiratory consumption of NADH is repressed. The other main non-respiratory mechanism to recycle NADH is to produce glycerol; ~ 14% of carbon entering glycolysis was routed to this side product. This $NADH/NAD^+$ flux is independent of the other cofactor pool, $NADPH/NADP^+$, which is used in several anabolic reactions including fatty acid biosynthesis (two NADPH are consumed per two carbons added to the growing fatty acid chain). Yeast maintain $[NAD^+]/[NADH] > > 1$, and $[NADP^+/NADPH] < 1$, such that the cofactor concentration gradients favor reduction of NAD^+ for $NADH/NAD^+$-dependent reactions, and oxidation of NADPH for $NADPH/NADP^+$-dependent reactions. Our reconstruction shows most NADPH being produced by ALD (~ 67%), with only a small amount (~ 25%) from the pentose phosphate pathway. The vast majority of all NADPH is consumed by GDH (~ 60%) and fatty acid biosynthesis (~ 40%). Altogether, on a basis of carbon entering from glucose, ~ 33% is routed to ethanol, ~ 20% to CO_2, ~ 14% to glycerol, ~ 2% to acetate, ~ 16% to biomass, and ~ 15% to fatty acid product. The full results of our metabolic flux reconstruction are available in Supplementary File 3.

The proteomics and flux results allowed us to identify possible bottlenecks or imbalances in our pathway. For example, that Ald6p is the predominant ALD isoform means flux through this reaction produces NADPH—rather than NADH if another ALD isoenzyme were prevalent. Following the carbon flux to our product, on a basis of one acetyl-CoA, the stoichiometry is 0.5x Glucose + 1.38x ATP + 1.25x NADPH - 1 NADH = 0.125x C_{16}FOH (ADP, $NADP^+$, NAD^+, H^+, and CO_2 not included for simplicity). Even though ALD flux produces NADPH, the metabolic route from glucose to fatty alcohol requires additional NADPH and produces excess NADH, an imbalance we sought to remediate (discussed in a later section). First, however, we focused on increasing carbon flux into fatty alcohol production by pull-push-block engineering: "pulling" on the pathway by overexpressing the terminal enzyme; "pushing" by overexpressing enzymes to overcome bottlenecks on the metabolic route to our product; and "blocking" unwanted consumption of products or intermediates by deleting genes catalyzing undesirable reactions (Tai and Stephanopoulos, 2013).

3.2. Pull: comparing fatty acyl-CoA reductase variants

To pull flux towards our product, first we focused on the only heterologous enzyme in our pathway, fatty acid reductase (FAR), which converts fatty acyl-CoA produced by fatty acid biosynthesis into fatty alcohols. Besides our earlier report expressing a *Mus musculus* FAR in *S. cerevisiae* (Runguphan and Keasling, 2013), other labs have reported on heterologously expressing a FAR from *Tyto alba* (Feng et al., 2015) and two from *Marinobacter hydrocarbonasticus* (Liu et al., 2013; Wahlen et al., 2009; Willis et al., 2011). To determine the variant most effective for fatty alcohol production in *S. cerevisiae*, we chromosomally integrated the four FAR coding sequences (*MmFAR1*, *TaFAR1*, *MaFAR2*, and *MaFAR7*, codon-optimized sequences in Suppl. Table 2) individually into our fatty acyl-CoA-overproducing strain WRY1, and compared fatty alcohol production using GC-MS (Fig. 2). Of the four

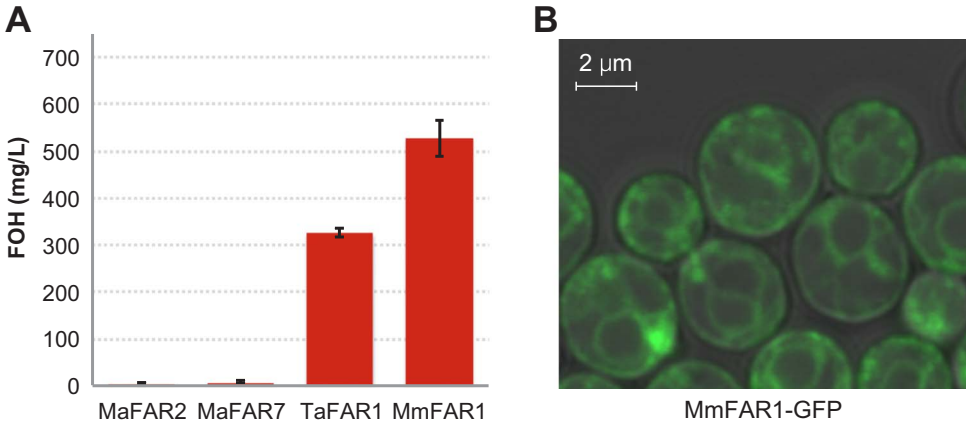

Fig. 2. Comparing four heterologous fatty acid reductases in *S. cerevisiae*. **(A)** Four FARs were chromosomally integrated into a fatty acyl-CoA overproducing strain (WRY1) and fatty alcohol production by the resulting strains was compared. Abbrev.: *MaFAR2*, *Maqu2220* from *Marinobacter aquaeoli*; *MaFAR7*, *Maqu2507* from the same organism; *TaFAR1*, *FAR1* from *Tyto alba*; *MmFAR1*, *FAR1* from *Mus musculus*. All four FARs were expressed from the same *208a* locus, *TEF1* promoter, and *CYC1* terminator. Cultures were grown in 5 ml YPD overlaid with 10% dodecane for three days. The bars represent the mean, and the error bars one standard deviation, for three to four biological replicates. **(B)** Confocal microscopy images of yL405 containing *MmFAR1-GFP* shows the fusion enzyme to be ER-localized, as are many native enzymes that use the same substrate fatty acyl-CoA (Natter et al., 2005).

enzymes, *MmFAR1* led to the highest titer at ~ 550 mg/L (mass of extracted fatty alcohols/aqueous culture volume). *TaFAR1* produced two thirds of that, and the two *Marinobacter* FARs negligible levels. *MmFAR1* produced mostly C16 fatty alcohols (87% C16, 7% C18, and 3% each C12 and C14), similar to the distribution from *TaFAR1*. The strain containing the best-performing *MmFAR1* gene (*208a::P_{TEF1}-FAR, acc1::P_{TEF1}-ACC1, fas1::P_{TEF1}-FAS1, fas2:: P_{TEF1}::FAS2*) is the base strain for all subsequent engineering and is henceforth referred to as yL405.

Having determined *MmFAR1* to be our best enzyme candidate for fatty alcohol production, we next overexpressed it further to investigate whether this reaction still limited production. Starting with yL405, we added a second *MmFAR1*—further referred to as "*FAR*", in a cassette containing the strongest promoter (from *GAL1*) and terminator (from *TDH1*) reported in recent studies (Lee et al., 2015; Reider Apel et al., 2016)— which increased fatty alcohol titer by 16 fold (Fig. 3A). In parallel, we added to yL405 a version of the second *FAR* fused at the C-terminus to a green fluorescent protein (GFP) to examine enzyme solubility and localization. Confocal microscopy showed GFP localization in a pattern typical of the endoplasmic reticulum (ER) common in lipid metabolic enzymes (Natter et al., 2005) (Fig. 2B). We did not find this localization problematic since many yeast enzymes that utilize fatty acyl-CoA as substrate (e.g., fatty acyl-CoA elongase Elo1p; desaturase Ole1p; acyl-CoA:sterol acyltransferases Are2p and Are1p) localize to the ER; and since MmFar1p produced high levels of fatty alcohols. However, since fatty acyl-CoA is produced in the cytoplasm, we wondered whether a soluble, cytoplasmic MmFar1p might access additional substrate and further increase titer. Since MmFar1p fused C-terminally to GFP maintained membrane localization, we hypothesized that the N-

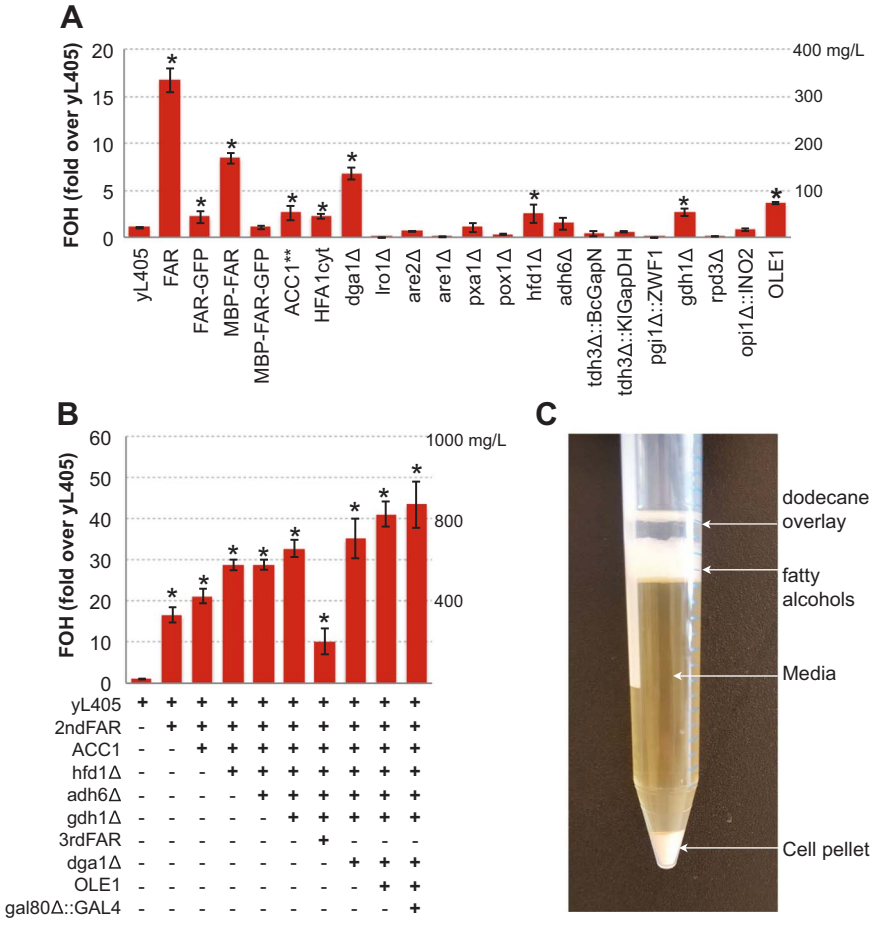

Fig. 3. Genetic modifications to improve fatty alcohol production. **(A)** Genetic modifications to yL405 (an acyl-CoA overproducing strain containing one copy of the best-performing *MmFAR1*) were screened in parallel for improvements to fatty alcohol production, with titer shown as a fraction of the parent yL405. FAR refers to an added copy of *MmFAR1* expressed from the strong *GAL1* promoter, with or without protein tag(s), as indicated. **(B)** Stacking beneficial single-gene edits leads to additional improvements in titer culminating in the highest producing strain yL434. **(C)** The high production level from yL434 results in precipitation of fatty alcohols from the saturated dodecane overlay. The bars represent the mean, and the error bars one standard deviation, for three to four biological replicates. Asterisks indicate strains with a statistically higher titer compared to strain yL405 ($p < 0.05$, student t-test). Cultures for panels A and B were grown in plastic 24-well plates containing 1 ml YPG overlaid with 20% dodecane for three days. The culture for panel C was grown in a 250-ml baffled flask containing 10 ml YPD overlaid with 20% dodecane for three days. These cultivation methods and that of Fig. 2 result in different titers (see Materials & Methods).

terminus might contain a membrane-targeting signal and that adding an N-terminal maltose binding protein (MBP) might result in a soluble fusion protein. We thus introduced either *MBP-FAR* or *MBP-FAR-GFP* (to verify localization) to yL405. However, the strain containing *MBP-FAR-GFP* did not show cytosolic GFP localization (Suppl. Fig. 1), and none of the fusion enzymes improved fatty alcohol production over an untagged second copy of *FAR* (Fig. 3A).

3.3. Push: overexpressing acetyl-CoA carboxylase variants

To push flux through potential bottlenecks, we next focused on the first committed—and limiting (Tehlivets et al., 2007)—step of fatty acid biosynthesis: the production of malonyl-CoA by acetyl-CoA carboxylase (ACC), in yeast encoded by *ACC1*. Although in our earlier work we introduced a strong promoter to drive *ACC1*, the present shotgun proteomics analysis detected much lower levels of Acc1p compared to Fas1p and Fas2p expressed from the same *TEF1* promoter. It is known that the gene product of *ACC1* is regulated post-transcriptionally, e.g., through phosphorylation sites that inhibit ACC1 activity. Recent work has shown that mutating two serine residues on Acc1p (S659A, S1157A) can produce high levels of malonyl-CoA-derived products (Shi et al., 2014). We therefore introduced into yL405 a second copy of *ACC1* containing these two mutations (*ACC1***) expressed from the strong *GAL1* promoter. In parallel, we constructed a cytosolic version of *S. cerevisiae*'s native mitochondrial ACC, *HFA1*, by replacing the latter's N-terminal mitochondrial targeting signal with the *ACC1* N-terminus (*HFA1cyt*). This fusion protein has been shown to rescue an *acc1*Δ phenotype (Hoja et al., 2004) and does not contain any Snf1p target sites, or presumably any other uncharacterized or indirect inactivation mechanisms since Hfa1p activity is required for proliferating mitochondria during respiration when Snf1p signaling is active. Both ACC proteins improved fatty alcohol production compared to yL405, with *ACC1*** leading to the best improvement at 2.6 fold.

3.4. Block: inhibiting reactions consuming fatty alcohols and intermediates

To block undesirable reactions, we deleted eight genes encoding enzymes that consume fatty acyl-CoA or fatty alcohols. These included enzymes that produce triacylglycerides (TAGs) for storage (*DGA1* and *LRO1*) or steryl esters (*ARE2* and *ARE1*), the peroxisomal importer (*PXA1*), the first step of beta-oxidation (*POX1*), and two that dehydrogenate fatty alcohols (*HFD1* and *ADH6*). We performed these deletions in parallel on the base strain yL405 and screened for fatty alcohol production. Of the resulting eight deletion strains, *dga1*Δ had the highest titer (at 6.8-fold higher than parent yL405 strain), followed by *hfd1*Δ (at 2.6-fold higher), then *adh6*Δ (at 1.5-fold higher). None of the other deletions led to any improvement in titer.

3.5. Optimizing NADPH/NADP+ and NADH/NAD+ cofactor usage

Besides pull-push-block engineering of carbon flux, we also focused balancing redox cofactor usage. As discussed above, the fatty alcohol pathway produces excess NADH and requires additional NADPH. To remediate this redox cofactor imbalance in our fatty alcohol pathway, first we considered replacing native NADH-producing GapDH with an NADPH-producing variant as has been pursued for other bioproducts (Guo et al., 2011; Kildegaard et al., 2016; Zhang et al., 2011). From our proteomics results, we found that of the three GapDH isoenzymes in yeast, Tdh3p was the most highly expressed. We thus replaced *TDH3* with either an NADPH-producing GapDH from *Kluyveromyces lactis* (*KlGapDH*) (Verho et al., 2002), or a non-phosphorylating GapDH from *Bacillus cereus* (*BcGapN*) (Guo et al., 2011) in the baseline yL405 strain. Neither resulting strain produced more fatty alcohols than the parent (Fig. 3A). We note that the reaction catalyzed by GapDH has a positive ΔG^0 = 1.5 kcal/mol (Stryer, 1988). Normally, a chemical driving force afforded by a high cellular [NAD^+]/[NADH] ratio makes the concentration-adjusted ΔG spontaneous. For an $NADP^+$-dependent reaction, however, the cofactor ratio is inverted ([$NADP^+$]/[NADPH] < 1) suggesting such a reaction might result in a bottleneck, or futile cycling between a forward, NADH-generating flux catabolized by the remaining native Tdh1p and Tdh2p, and a reverse, NADPH-consuming flux catabolized by KlGapdhp. The reaction catalyzed by BcGapNp, on the other hand, has a very favorable ΔG^0, but skips the ATP-generating step that normally follows GapDH, thus creating a pathway ATP deficit. Similar thermodynamic considerations stemming from concentration gradients across the redox cofactor pairs are relevant to other pathways.

Next, we sought to increase NADPH availability for fatty acid biosynthesis. Our flux reconstruction indicated that the fatty acid pathway consumes only ~ 5% of cellular ATP, but 40% of cellular NADPH, suggesting the latter cofactor may limit production. The quantitative analysis further showed that (1) carbon flux through the NADPH-producing pentose phosphate pathway is only 2% of that through PGI, (2) Pgi1p is expressed highly, and (3) Zwf1p—the first and limiting enzyme of the pentose phosphate—was undetectable even though downstream pentose phosphate enzymes were detected. Thus, we attempted to force flux through the pentose phosphate pathway by deleting *PGI1* and in its place overexpressing *ZWF1* (*pgi1*Δ*::ZWF1*), also in the yL405 strain. However, the resulting strain grew slowly and barely produced any fatty alcohols (Fig. 3A).

Lastly, we attempted to minimize NADPH consumed by competing reactions. Our flux analysis indicated that 60% of all NADPH is consumed to produce glutamate (from alpha-ketoglutarate and ammonia) with the two isoenzymes catabolizing this reaction, Gdh1p and Gdh3p, expressed at 0.12% and 0.034% of soluble protein, respectively. We theorized that deleting *GDH1* might slow down glutamate biosynthesis and free up NADPH for fatty acid biosynthesis, as well as carbon. We thus introduced a *gdh1*Δ deletion into yL405, resulting in a 2.7-fold improvement in fatty alcohol production.

3.6. Perturbations to fatty acid regulation

The fatty acid pathway is energy intensive and regulated at several levels (Tehlivets et al., 2007). Some of our strategies address known levels of regulation—e.g., using a strong constitutive promoter to overexpress *ACC1*, *FAS1*, and *FAS2*; or abolishing post-translational phosphorylation sites on *ACC1*—yet additional known or unknown regulatory mechanisms may continue to limit pathway flux. A recent study showed that deleting a histone deacetylase encoded by *RPD3* dramatically increased fatty alcohol production from an *S. cerevisiae* strain expressing *TaFAR1* (Feng et al., 2015). In yL405, *rpd3*Δ did not yield any improvement (Fig. 3A). We also deleted the gene encoding the negative regulator of fatty acid biosynthesis, *OPI1*, and in its place overexpressed the positive regulator encoded by *INO2* in yL405. However, the *opi1*Δ*::INO2* replacement did not improve fatty alcohol titers (Fig. 3A).

Lastly, we were intrigued to read a report that found (1) a correlation in mammalian tissues between lipid accumulation (as TAGs) and expression level of Δ9-desaturase (which produces mono-unsaturated fatty acyl-CoA), and (2) that overexpression of Δ9-desaturase in *Yarrowia lipolitica* led to dramatically increased levels of TAGs in an engineered strain (Qiao et al., 2015). To explore the possibility of Δ9-desaturase increasing flux through our fatty alcohol pathway in *S. cerevisiae*—by increasing membrane fluidity and access of MmFar1p to substrate (Degreif et al., 2017), or through an indirect feedback inhibition as in other organisms (Zhang et al., 2012)—we overexpressed the native *S. cerevisiae* Δ9-desaturase (encoded by *OLE1*) in yL405, resulting in a 4-fold improvement in fatty alcohol titer (Fig. 3A).

3.7. Combining beneficial genetic edits into highest-producing strain

Having found several genetic modifications that improved fatty alcohol titers, we next stacked beneficial changes into a high-producing

strain. Starting with the best single-edit strain containing a second copy of *FAR*, we then added *ACC1***, resulting in an additional 4.6-fold improvement over yL405 (Fig. 3B). We then stacked deletions of *hfd1*Δ, *adh6*Δ, and *gdh1*Δ, increasing titer up to 32.7-fold above yL405. Because a second copy of *FAR* led to the most dramatic improvement in titer in our single-gene edit strains, we added a third copy to examine whether FAR activity remained limiting, but found the resulting strain produced less than parent (Fig. 3B). Instead, we combined the remaining beneficial single-gene edits *dga1*Δ and *OLE1* to reach a titer 40-fold higher than yL405.

Lastly, we sought to deregulate the *GAL1* promoter driving *MmFAR* and *ACC1*** by deleting the negative regulator of galactose metabolism (*GAL80*) and in its place introducing a copy of the positive regulator (*GAL4*). This perturbation in galactose metabolism has the advantage of making the *GAL1* promoter constitutively active in glucose, allowing us to achieve high production using this inexpensive sugar as the carbon source. Our final yL434 strain, containing two copies of *MmFAR1*, *ACC1***, deletions of *dga1*Δ, *hfd1*Δ, *adh6*Δ, and *gdh1*Δ, overexpression of *OLE1*, and a *gal80*Δ*::GAL4* replacement produced 43-fold more fatty alcohols than the original yL405 strain (Fig. 3B). At this level of production, we observed precipitation of fatty alcohols from the saturated dodecane overlay in yL434 cultures (Fig. 3C).

3.8. Fatty alcohol production from biomass sugars released using renewable ionic liquids

Having demonstrated a high-producing strain, we turned to evaluating production from lignocellulosic feedstocks derived from non-food bioenergy crops. Specific combinations of anions and cations that are liquids at room temperature (termed "ionic liquids", ILs) have been shown to deconstruct plant biomass, allowing for subsequent enzymatic de-polymerization to free constituent sugars (Zhu et al., 2006). However, these processes are limited by high costs of conventional ILs, water usage, and toxicity. Recently, attention has shifted to ILs derived from benign cholinium cations stabilized with readily available bio-based anions (Petkovic et al., 2010; Sun et al., 2016). A recently demonstrated one-pot process involving biomass pretreatment with ILs composed of cholinium and amino acids followed by enzymatic saccharification requires minimal water and unit operations, thus dramatically lowering process costs (F. Xu et al., 2016).

To examine the feasibility of using lignocellulosic feedstocks to produce fatty alcohols, we pretreated two types of non-food crops (switchgrass and sorghum) with cholinium-based ILs containing three common bio-based anions (lysinate, alpha-ketoglutarate, or aspartate) in a one-pot process (see Materials and Methods). The six resulting biomass hydrolysate media all contained ~ 1% glucose, and all produced more than 150 mg/L fatty alcohols using the baseline strain yL405 (Supplementary Fig. S2). The biomass hydrolysate media derived from sorghum pretreated with cholinium aspartate produced the most, at 400 mg/L fatty alcohols, and is further referred to as YPBiomass. We then grew the highest producing yL434 strain in YPBiomass (as well as traditional rich media YPD and YPG) in baffled flasks, finding in preliminary experiments that greater aeration lead to improved production. Fatty alcohol levels reached 0.7 g/L in YPBiomass, corresponding to ~ 0.06 g/g-glucose, already above the highest reported titers and yields (in shake flasks) using any media (Zhou et al., 2016). In YPD medium, fatty alcohol production reached 1.2 g/L and 0.07 g/g-glucose (Fig. 4), corresponding to ~ 20% of the maximum theoretical yield, well above all previous reports of fatty alcohol production in *S. cerevisiae*.

3.9. Fed-batch bioreactor fermentations

Finally, we turned to maximizing titer and demonstrating scale-up in fed-batch fermentation. Previous work on *S. cerevisiae* has suggested maximal yields depend on a balance between feeding enough sugar to maintain high product flux, but not too much as to induce overflow metabolism (Mazzoleni et al., 2015). To that end, we set up 2-L scale bioreactors with feed strategies aimed at minimizing overflow metabolism and maximizing titer. For all four bioreactors, we cultured yL434 in an initial 1-L YPD in batch operation until glucose depletion (as indicated by O_2 spike), and then added concentrated glucose following different feed strategies: bioreactor A contained half the normal glucose concentration in batch phase (1% vs. 2% for others) and was fed a constant ~ 1.5 g/h concentrated glucose; bioreactor B was pulse-fed ~ 1 g/h (as ~ 1 g pulses of concentrated glucose upon carbon source depletion as indicated by a spike in O_2 concentration in the bioreactor occurring every ~ 1 h); bioreactor C a constant ~ 3 g/h; and bioreactor D a constant ~ 1.5 g/h. All four bioreactors reached ODs of 25–31 and fatty alcohol titers > 3 g/L and were still climbing at the end of the allotted 9-day fermentation time (Fig. 5A-D). Bioreactor A showed the greatest rate of fatty alcohol production in fed-batch phase, the highest final titer, and the lowest feed consumption, with the overlay showing extensive precipitation of fatty alcohols (Supplementary Fig. S3). The final titer was 6 g/L, and the yield 58 mg/g-glucose, corresponding to 20% of the maximum theoretical yield.

4. Conclusions

In the present work, we engineered *S. cerevisiae* for high-level production of fatty alcohols guided by quantitative analysis of global protein expression and flux modeling. We compared four heterologous fatty acid reductases, finding high activity and ER localization from a *Mus musculus* FAR. After screening an additional 21 single-gene edits, we identified the following successful strategies to improve titer: (1) increasing expression of *MmFAR1*, (2) deleting competing reactions encoded by *DGA1*, *HFD1*, and *ADH6*, (3) overexpressing a mutant of the bottleneck enzyme encoded by *ACC1* insensitive to post-transcriptional and post-translational repression, (4) limiting NADPH and carbon flux to glutamate biosynthesis by deleting the enzyme encoded by *GDH1*, and (5) limiting fatty acid pathway repression by overexpressing the desaturase encoded by *OLE1*. Our final strain containing eleven genetic modifications compared to the parent BY4741 strain produced 1.2 g/L fatty alcohols in shake flasks.

Our work complements research in production of fatty acid-derived products in other microbial hosts in several ways (Liu et al., 2013; Teixeira et al., 2017). The findings about the ER subcellular localization of MmFar1p (mouse fatty acid reductase) is relevant to engineering pathway compartmentalization as a way to optimize bioproduction or tailor product distribution (Avalos et al., 2013; Sheng et al., 2016; P. Xu et al., 2016). Our observation that overexpression of a fatty acid desaturase led to improvements in fatty acid products in *S. cerevisiae* as in *Y. lipolytica* (Qiao et al., 2015) points to commonalities in fatty pathway engineering in both organisms. Recently, oleaginous yeasts such as *Y. lipolytica* and *Rhodosporidium toruloides* have emerged as promising candidates for fatty acid pathway engineering (Fillet et al., 2015; Wang et al., 2016; P. Xu et al., 2016). In general, these oleaginous organisms are less genetically tractable than *S. cerevisiae*, such that rapidly identifying candidate engineering targets in *S. cerevisiae* can facilitate further improving fatty chemical bioproduction in oleaginous hosts.

We also demonstrated high-level production from feedstocks produced from non-food crops and cholinium-based renewable bionic ILs, reaching a titer of 0.7 g/L in shake flasks. Lastly, we demonstrated scale-up fermentation and explored alternative feeding strategies aimed at limiting overflow metabolism, achieving a titer of 6.0 g/L in a 2-L, fed-batch bioreactor. These titers are the highest for fatty alcohols reported to date for *S. cerevisiae*. To our knowledge, this is also the first report of a bioproduct produced by yeast from feedstocks derived solely from biomass.

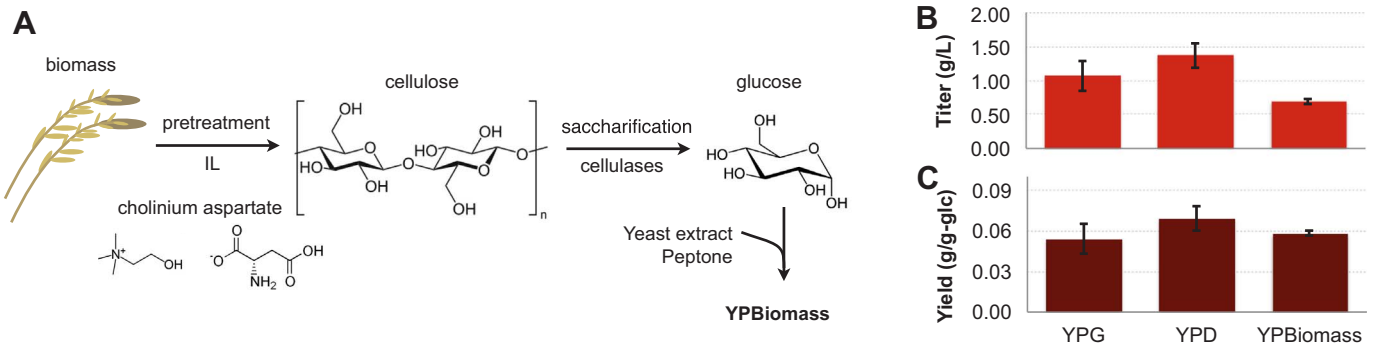

Fig. 4. Fatty alcohol production from lignocellulosic biomass. (A) Biomass pretreatment with ionic liquids (ILs) containing cholinium cation paired with bio-based anions, e.g., aspartate, break down lignocellulose to be depolymerized using cellulase enzymes to free constituent sugars. **(B)** The highest producing yL434 strain grown in biomass hydrolysates media (YPBiomass) or conventional rich (YPD or YPG) media produces high levels and **(C)** yields of fatty alcohols. Cultures were grown in plastic 250-ml baffled flasks containing 10 ml medium overlaid with 20% dodecane for three days. The bars represent the mean, and the error bars one standard deviation, for three replicates.

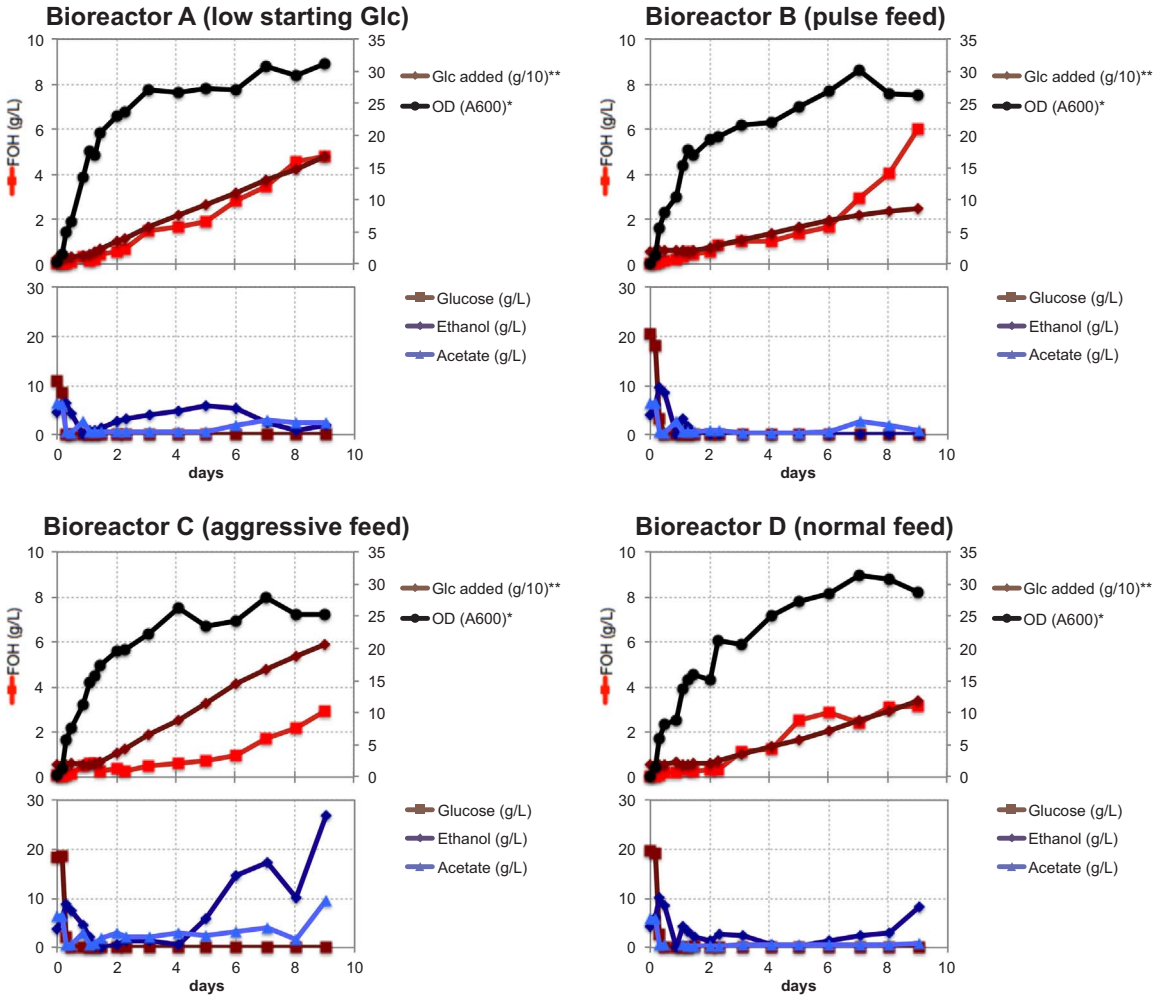

Fig. 5. High-density, fed-batch bioreactor fermentations. The highest producing yL434 strain was grown in 2 L-scale bioreactors under different fed-batch conditions to maximize titer. **(A)** Bioreactor A contained half the normal glucose concentration in batch phase (1% vs. 2% for others) and was fed a constant ~ 1.5 g/h concentrated glucose. **(B)** Bioreactor B was pulse-fed ~ 1 g/h (1 g pulses of concentrated glucose upon carbon source depletion as indicated by O_2 spike, occurring every ~ 1 h). **(C)** Bioreactor C was fed a constant ~ 3 g/h. **(D)** Bioreactor D was fed a constant ~ 1.5 g/h. *OD values were plotted on the scale on the right. **Mass of glucose added was also plotted on the right, divided by 10, such that the maximum value of 35 on the scale indicates 350 g of glucose.

Conflict of interest

JDK has financial interests in Amyris, Lygos, Constructive Biology, and Demetrix.

Acknowledgements

This work was part of the DOE Joint BioEnergy Institute (www.jbei.org) supported by the United States Department of Energy (DOE), Office of Science, Office of Biological and Environmental Research, through contract DE-AC02-05CH11231 between Lawrence Berkeley

National Laboratory and the DOE. The US Government retains and the publisher, by accepting the article for publication, acknowledges that the US Government retains a non-exclusive, paid-up, irrevocable, worldwide license to publish or reproduce the published form of this manuscript, or allow others to do so, for US Government purposes. The DOE will provide public access to these results of federally sponsored research in accordance with the DOE Public Access Plan (energy.gov/downloads/doe-public-access-plan). We thank Eric Sundstrom, Mona Misriaghi, and Fabrice Masson at the DOE ABPDU for technical assistance with bioreactor experiments.

Appendix A. Supporting information

Supplementary data associated with this article can be found in the online version at http://dx.doi.org/10.1016/j.ymben.2017.06.004.

References

Avalos, J.L., Fink, G.R., Stephanopoulos, G., 2013. Compartmentalization of metabolic pathways in yeast mitochondria improves the production of branched-chain alcohols. Nat. Biotechnol. 31, 335–341. http://dx.doi.org/10.1038/nbt.2509.

Batth, T.S., Keasling, J.D., Petzold, C.J., 2012. Targeted proteomics for metabolic pathway optimization. In: Fungal Secondary Metabolism: Methods and Protocols, Methods in Molecular Biology. Vol. 944. pp. 47–58. http://dx.doi.org/10.1007/978-1-62703-122-6.

Brachmann, C.B., Davies, A., Cost, G.J., Caputo, E., Li, J., Hieter, P., Boeke, J.D., 1998. Designer deletion strains derived from Saccharomyces cerevisiae S288C: a useful set of strains and plasmids for PCR-mediated gene disruption and other applications. Yeast 14, 115–132. http://dx.doi.org/10.1002/(SICI)1097-0061(19980130)14:2 < 115::AID-YEA204 > 3.0.CO;2-2.

Caspeta, L., Nielsen, J., 2013. Economic and environmental impacts of microbial biodiesel. Nat. Biotechnol. 31, 789–793. http://dx.doi.org/10.1038/nbt.2683.

Clomburg, J.M., Blankschien, M.D., Vick, J.E., Chou, A., Kim, S., Gonzalez, R., 2015. Integrated engineering of β-oxidation reversal and ω-oxidation pathways for the synthesis of medium chain ω-functionalized carboxylic acids. Metab. Eng. 28, 202–212. http://dx.doi.org/10.1016/j.ymben.2015.01.007.

Connor, R., Uhlenbrook, S., 2016. The United Nations World Water Development Report 2016. Paris, France.

Degreif, D., de Rond, T., Bertl, A., Keasling, J.D., Budin, I., 2017. Lipid engineering reveals regulatory roles for membrane fluidity in yeast flocculation and oxygen-limited growth. Metab. Eng. 41, 46–56. http://dx.doi.org/10.1016/j.ymben.2017.03.002.

Feng, X., Lian, J., Zhao, H., 2015. Metabolic engineering of Saccharomyces cerevisiae to improve 1-hexadecanol production. Metab. Eng. 27, 10–19. http://dx.doi.org/10.1016/j.ymben.2014.10.001.

Fillet, S., Gibert, J., Suárez, B., Lara, A., Ronchel, C., Adrio, J.L., 2015. Fatty alcohols production by oleaginous yeast. J. Ind. Microbiol. Biotechnol. 42, 1463–1472. http://dx.doi.org/10.1007/s10295-015-1674-x.

Gaikwad, S., 2016. Fatty Alcohol Market Size, Industry Analysis Report: Forecast, 2016–2023. Ocean View, DE.

García Martín, H., Kumar, V.S., Weaver, D., Ghosh, A., Chubukov, V., Mukhopadhyay, A., Arkin, A., Keasling, J.D., 2015. A method to constrain genome-scale models with 13C labeling data. PLOS Comput. Biol. 11, e1004363. http://dx.doi.org/10.1371/journal.pcbi.1004363.

Ghosh, A., Ando, D., Gin, J., Runguphan, W., Denby, C., Wang, G., Baidoo, E.E.K., Shymansky, C., Keasling, J.D., García Martín, H., 2016. (13)C metabolic flux analysis for systematic metabolic engineering of S. cerevisiae for overproduction of fatty acids. Front. Bioeng. Biotechnol. 4, 76. http://dx.doi.org/10.3389/fbioe.2016.00076.

Gietz, R.D., Woods, R.A., 2002. Transformation of yeast by lithium acetate/single-stranded carrier DNA/polyethylene glycol method. Methods Enzymol. 350, 87–96.

Goh, E.-B., Baidoo, E.E.K., Keasling, J.D., Beller, H.R., 2012. Engineering of bacterial methyl ketone synthesis for biofuels. Appl. Environ. Microbiol. 78, 70–80. http://dx.doi.org/10.1128/AEM.06785-11.

Guo, Z., Zhang, L., Ding, Z., Shi, G., 2011. Minimization of glycerol synthesis in industrial ethanol yeast without influencing its fermentation performance. Metab. Eng. 13, 49–59. http://dx.doi.org/10.1016/j.ymben.2010.11.003.

Haushalter, R.W., Kim, W., Chavkin, T.A., The, L., Garber, M.E., Nhan, M., Adams, P.D., Petzold, C.J., Katz, L., Keasling, J.D., 2014. Production of anteiso-branched fatty acids in Escherichia coli; next generation biofuels with improved cold-flow properties. Metab. Eng. 26C, 111–118. http://dx.doi.org/10.1016/j.ymben.2014.09.002.

Hoja, U., Marthol, S., Hofmann, J., Stegner, S., Schulz, R., Meier, S., Greiner, E., Schweizer, E., 2004. HFA1 encoding an organelle-specific acetyl-CoA carboxylase controls mitochondrial fatty acid synthesis in Saccharomyces cerevisiae. J. Biol. Chem. 279, 21779–21786. http://dx.doi.org/10.1074/jbc.M401071200.

Kalscheuer, R., Stölting, T., Steinbüchel, A., 2006. Microdiesel: Escherichia coli engineered for fuel production. Microbiology 152, 2529–2536. http://dx.doi.org/10.1099/mic.0.29028-0.

Kildegaard, K.R., Jensen, N.B., Schneider, K., Czarnotta, E., Ozdemir, E., Klein, T., Maury, J., Ebert, B.E., Christensen, H.B., Chen, Y., Kim, I.K., Herrgard, M.J., Blank, L.M., Forster, J., Nielsen, J., Borodina, I., 2016. Engineering and systems-level analysis of Saccharomyces cerevisiae for production of 3-hydroxypropionic acid via malonyl-CoA reductase-dependent pathway. Microb. Cell Fact. 15, 13. http://dx.doi.org/10.1186/s12934-016-0451-5.

Lee, M.E., DeLoache, W.C., Cervantes, B., Dueber, J.E., 2015. A highly-characterized yeast toolkit for modular, multi-part assembly. ACS Synth. Biol. http://dx.doi.org/10.1021/sb500366v.

Liu, A., Tan, X., Yao, L., Lu, X., 2013. Fatty alcohol production in engineered E. coli expressing Marinobacter fatty acyl-CoA reductases. Appl. Microbiol. Biotechnol. 97, 7061–7071. http://dx.doi.org/10.1007/s00253-013-5027-2.

Liu, Y., Chen, S., Chen, J., Zhou, J., Wang, Y., Yang, M., Qi, X., Xing, J., Wang, Q., Ma, Y., 2016. High production of fatty alcohols in Escherichia coli with fatty acid starvation. Microb. Cell Fact. 15, 129. http://dx.doi.org/10.1186/s12934-016-0524-5.

Mazzoleni, S., Landi, C., Cartenì, F., de Alteriis, E., Giannino, F., Paciello, L., Parascandola, P., 2015. A novel process-based model of microbial growth: self-inhibition in Saccharomyces cerevisiae aerobic fed-batch cultures. Microb. Cell Fact. 14, 109. http://dx.doi.org/10.1186/s12934-015-0295-4.

Mo, M.L., Palsson, B.Ø., Herrgård, M.J., 2009. Connecting extracellular metabolomic measurements to intracellular flux states in yeast. BMC Syst. Biol. 3, 37. http://dx.doi.org/10.1186/1752-0509-3-37.

Montague, T.G., Cruz, J.M., Gagnon, J.A., Church, G.M., Valen, E., 2014. CHOPCHOP: a CRISPR/Cas9 and TALEN web tool for genome editing. Nucleic Acids Res. 42, 401–407. http://dx.doi.org/10.1093/nar/gku410.

Natter, K., Leitner, P., Faschinger, A., Wolinski, H., McCraith, S., Fields, S., Kohlwein, S.D., 2005. The spatial organization of lipid synthesis in the yeast Saccharomyces cerevisiae derived from large scale green fluorescent protein tagging and high resolution microscopy. Mol. Cell. Proteom. 4, 662–672. http://dx.doi.org/10.1074/mcp.M400123-MCP200.

Petkovic, M., Ferguson, J.L., Gunaratne, H.Q.N., Ferreira, R., Leitão, M.C., Seddon, K.R., Rebelo, L.P.N., Pereira, C.S., Pereira, C.S., Ferreira, R., Seddon, K.R., Rebelo, L.P.N., Pereira, C.S., 2010. Novel biocompatible cholinium-based ionic liquids—toxicity and biodegradability. Green Chem. 12, 643. http://dx.doi.org/10.1039/b922247b.

Pfleger, B.F., Gossing, M., Nielsen, J., 2015. Metabolic engineering strategies for microbial synthesis of oleochemicals. Metab. Eng. 29, 1–11. http://dx.doi.org/10.1016/j.ymben.2015.01.009.

Qiao, K., Imam Abidi, S.H., Liu, H., Zhang, H., Chakraborty, S., Watson, N., Kumaran Ajikumar, P., Stephanopoulos, G., 2015. Engineering lipid overproduction in the oleaginous yeast Yarrowia lipolytica. Metab. Eng. 29, 56–65. http://dx.doi.org/10.1016/j.ymben.2015.02.005.

Reider Apel, A., D'Espaux, L., Wehrs, M., Sachs, D., Li, R.A., Tong, G.J., Garber, M., Nnadi, O., Zhuang, W., Hillson, N.J., Keasling, J.D., Mukhopadhyay, A., 2016. A Cas9-based toolkit to program gene expression in Saccharomyces cerevisiae. Nucleic Acids Res. 1–14. http://dx.doi.org/10.1093/gbe/evw245.

Runguphan, W., Keasling, J.D., 2013. Metabolic engineering of saccharomyces cerevisiae for production of fatty acid-derived biofuels and chemicals. Metab. Eng. 21, 103–113. http://dx.doi.org/10.1016/j.ymben.2013.07.003.

Sheng, J., Stevens, J., Feng, X., 2016. Pathway compartmentalization in peroxisome of Saccharomyces cerevisiae to produce versatile medium chain fatty alcohols. Nat. Publ. Gr. http://dx.doi.org/10.1038/srep26884.

Shi, S., Chen, Y., Siewers, V., 2014. Improving production of malonyl coenzyme A-derived metabolites. mBio 5, e01130–14. http://dx.doi.org/10.1128/mBio.01130-14.Editor.

Stryer, L., 1988. Biochemistry. W.H. Freeman.

Sun, J., Konda, N.V.S.N.M., Shi, J., Parthasarathi, R., Dutta, T., Xu, F., Scown, C.D., Simmons, B.A., Singh, S., Andre, B., Arkin, A.P., Astromoff, A., Bakkoury, M. El, Bangham, R., Benito, R., Brachat, S., Campanaro, S., Curtiss, M., Davis, K., Deutschbauer, A., Entian, K.D., Flaherty, P., Foury, F., Garfinkel, D.J., Gerstein, M., Gotte, D., Guldener, U., Hegemann, J.H., Hempel, S., Herman, Z., Jaramillo, D.F., Kelly, D.E., Kelly, S.L., Kotter, P., LaBonte, D., Lamb, D.C., Lan, N., Liang, H., Liao, H., Liu, L., Luo, C.Y., Lussier, M., Mao, R., Menard, P., Ooi, S.L., Revuelta, J.L., Roberts, C.J., Rose, M., Ross-Macdonald, P., Scherens, B., Schimmack, G., Shafer, B., Shoemaker, D.D., Sookhai-Mahadeo, S., Storms, R.K., Strathern, J.N., Valle, G., Voet, M., Volckaert, G., Wang, C.Y., Ward, T.R., Wilhelmy, J., Winzeler, E.A., Yang, Y.H., Yen, G., Youngman, E., Yu, K.X., Bussey, H., Boeke, J.D., Snyder, M., Philippsen, P., Davis, R.W., Johnston, M., 2016. CO_2 enabled process integration for the production of cellulosic ethanol using bionic liquids. Energy Environ. Sci. 9, 2822–2834. http://dx.doi.org/10.1039/C6EE00913A.

Tai, M., Stephanopoulos, G., 2013. Engineering the push and pull of lipid biosynthesis in oleaginous yeast Yarrowia lipolytica for biofuel production. Metab. Eng. 15, 1–9. http://dx.doi.org/10.1016/j.ymben.2012.08.007.

Tehlivets, O., Scheuringer, K., Kohlwein, S.D., 2007. Fatty acid synthesis and elongation in yeast. Biochim. Biophys. Acta 1771, 255–270. http://dx.doi.org/10.1016/j.bbalip.2006.07.004.

Teixeira, P.G., Ferreira, R., Zhou, Y.J., Siewers, V., Nielsen, J., 2017. Dynamic regulation of fatty acid pools for improved production of fatty alcohols in Saccharomyces cerevisiae. Microb. Cell Fact. 1–11. http://dx.doi.org/10.1186/s12934-017-0663-3.

Thomas, D., Cherest, H., Surdin-Kerjan, Y., 1991. Identification of the structural gene for glucose-6-phosphate dehydrogenase in yeast. Inactivation leads to a nutritional requirement for organic sulfur. EMBO J. 10, 547–553.

Verho, R., Richard, P., Jonson, P.H., Sundqvist, L., Londesborough, J., Penttilä, M., 2002. Identification of the first fungal NADP-GAPDH from Kluyveromyces lactis. Biochemistry 41, 13833–13838. http://dx.doi.org/10.1021/bi0265325.

Wahlen, B.D., Oswald, W.S., Seefeldt, L.C., Barney, B.M., 2009. Purification, characterization, and potential bacterial wax production role of an NADPH-dependent fatty aldehyde reductase from Marinobacter aquaeolei VT8. Appl. Environ. Microbiol. 75, 2758–2764. http://dx.doi.org/10.1128/AEM.02578-08.

Wang, G., Xiong, X., Ghogare, R., Wang, P., Meng, Y., Chen, S., 2016. Biotechnology for biofuels exploring fatty alcohol – producing capability of Yarrowia lipolytica. Biotechnol. Biofuels 1–10. http://dx.doi.org/10.1186/s13068-016-0512-3.

Willis, R.M., Wahlen, B.D., Seefeldt, L.C., Barney, B.M., 2011. Characterization of a fatty acyl-CoA reductase from Marinobacter aquaeolei VT8: a bacterial enzyme catalyzing the reduction of fatty acyl-CoA to fatty alcohol. Biochemistry 50, 10550–10558. http://dx.doi.org/10.1021/bi2008646.

Xu, F., Sun, J., Konda, N.V.S.N.M., Shi, J., Dutta, T., Scown, C.D., Simmons, B.A., Singh, S., 2016a. Transforming biomass conversion with ionic liquids: process intensification and the development of a high-gravity, one-pot process for the production of cellulosic ethanol. Energy Environ. Sci. 9, 1042–1049. http://dx.doi.org/10.1039/C5EE02940F.

Xu, P., Qiao, K., Suk, W., Stephanopoulos, G., 2016. Engineering Yarrowia Lipolytica as a Platform for Synthesis of Drop-in Transportation Fuels and Oleochemicals. 113. http://dx.doi.org/10.1073/pnas.1607295113.

Zampar, G.G., Kümmel, A., Ewald, J., Jol, S., Niebel, B., Picotti, P., Aebersold, R., Sauer, U., Zamboni, N., Heinemann, M., 2013. Temporal system-level organization of the switch from glycolytic to gluconeogenic operation in yeast. Mol. Syst. Biol. 9, 651. http://dx.doi.org/10.1038/msb.2013.11.

Zhang, F., Ouellet, M., Batth, T.S., Adams, P.D., Petzold, C.J., Mukhopadhyay, A., Keasling, J.D., 2012. Enhancing fatty acid production by the expression of the regulatory transcription factor FadR. Metab. Eng. 14, 653–660. http://dx.doi.org/10.1016/j.ymben.2012.08.009.

Zhang, L., Tang, Y., Guo, Z., Ding, Z., Shi, G., 2011. Improving the ethanol yield by reducing glycerol formation using cofactor regulation in Saccharomyces cerevisiae. Biotechnol. Lett. 33, 1375–1380. http://dx.doi.org/10.1007/s10529-011-0588-6.

Zhou, Y.J., Buijs, N.A., Zhu, Z., Qin, J., Siewers, V., Nielsen, J., 2016. Production of fatty acid-derived oleochemicals and biofuels by synthetic yeast cell factories. Nat. Commun. 7, 11709. http://dx.doi.org/10.1038/ncomms11709.

Zhu, S., Wu, Y., Chen, Q., Yu, Z., Wang, C., Jin, S., Ding, Y., Wu, G., Tu, S., Xue, Y., 2006. Dissolution of cellulose with ionic liquids and its application: a mini-review. Green Chem. 8, 325. http://dx.doi.org/10.1039/b601395c.